



Genetic algorithm-powered non-sequential dwell time optimization for large optics fabrication

HYUKMO KANG,¹ TIANYI WANG,²  HEEJOO CHOI,^{1,3} AND
DAEWOOK KIM^{1,3,4,*}

¹Wyant College of Optical Sciences, University of Arizona, 1630 E. University Blvd., Tucson, AZ 85721, USA

²National Synchrotron Light Source II (NSLS-II), Brookhaven National Laboratory, PO Box 5000, Upton, New York 11973, USA

³Large Binocular Telescope Observatory, University of Arizona, 933 N. Cherry Ave., Tucson, AZ 85721, USA

⁴Department of Astronomy and Steward Observatory, University of Arizona, 933 N. Cherry Ave., Tucson, AZ 85721, USA

*dkim@optics.arizona.edu

Abstract: Computer Controlled Optical Surfacing (CCOS) is widely applied for fabricating large aspheric optical surfaces. For large optics fabrication, various sizes of polishing tools are used sequentially. This raises the importance of efficient and globally optimized dwell time map of each tool. In this study, we propose a GENetic Algorithm-powered Non-Sequential (GEANS) optimization technique to improve the feasibility of the conventional non-sequential optimization technique. GEANS consists of two interdependent parts: i) compose an influence matrix by imposing constraints on adjacent dwell points and ii) induce the desired dwell time map through the genetic algorithm. CCOS simulation results show that GEANS generates a preferable dwell time map that provides high figuring efficiency and structural similarity with the shape of target removal map, while improving computational efficiency more than 1000 times over the conventional non-sequential optimization method. The practicability of GEANS is demonstrated through error analyses. Random tool positioning error and tool influence function errors are imposed on dwell time maps. Compared to the conventional non-sequential optimization method, the power spectral density values of residual surface error from GEANS remain stable. GEANS also shows superior applicability when the maximum acceleration of a tool is applied.

© 2022 Optica Publishing Group under the terms of the [Optica Open Access Publishing Agreement](#)

1. Introduction

Since Computer Controlled Optical Surfacing (CCOS) developed, it has been widely applied for large aspheric optical surface fabrication [1–8]. The next generation telescope projects, such as Giant Magellan Telescope (GMT) [9], Thirty Meter Telescope (TMT) [10], and Extremely Large Telescope (ELT) [11,12] are required to meet the challenge of manufacturing off-axis segments. These projects contain from seven to several hundreds of meter-class segmented aspheric mirrors, so the advanced CCOS process must be efficient while accomplishing high precision optical surfaces.

In the CCOS process, dwell time calculation is an essential procedure. It deterministically guides the motion of machine tools at successive dwell points to remove material from an optical surface. In the past few decades, researchers have studied dwell time calculation algorithms which can be categorized into iterative algorithms [13,14], Fourier transform-based algorithms [15–17], matrix-based algorithms [18–24], and Bayesian-based algorithms [25]. These algorithms aim to obtain non-negative and smooth dwell time solutions that minimize the estimated residual errors of the optical surface. In the CCOS process of large optics fabrication, such as the CCOS platform for GMT fabrication at The University of Arizona, multiple tools with different sizes

and tool paths are utilized for a single workpiece [26–28] to correct the surface errors for various spatial frequencies. The tool path parameters, such as the machining interval and the path type (raster path, spiral path, random path, *etc.*), usually vary depending on the shape of the workpiece and the physical constraints of the machine tools. Therefore, the matrix-based methods are preferred in our CCOS process since the dwell time can be flexibly calculated for arbitrary dwell positions. Also, to improve the overall processing efficiency, the dwell time is expected to be calculated for multiple tools in the planning phase, and the metrology is only performed after all the tools complete their assigned works.

The dwell time for multiple tools was mostly optimized sequentially until the Non-Sequential dwell time optimization method (NS) was proposed in our previous research [19]. The NS method considers multiple Tool Influence Functions (TIFs) simultaneously in a single optimization run, which implicitly adds the necessary regularization to stabilize the linear solver. Therefore, it balances the dwell time for each tool and reduces the generation of mid-spatial-frequency errors effectively, which is a common issue in the sequential matrix-based methods. The results from the Conventional NS (CNS) are mathematically ideal and show high figuring efficiency in terms of the estimated residual errors. However, they have limitations in practical application. First, in terms of accuracy, CNS considers neither the Computer Numerical Control (CNC) hardware limitations (*i.e.*, the maximum local slope of the dwell time between each two consecutive dwell points) nor the practical preference that the dwell time map should smoothly resemble the shape of the target removal map in order to minimize any mid-to-high spatial frequency residual errors. Furthermore, in terms of computational efficiency, the increased size of the influence function matrix due to multiple TIFs brings heavier computational burden and makes iterative optimization difficult.

In this study, we proposed a GENetic Algorithm-powered Non-Sequential (GEANS) dwell time optimization method which enhances the feasibility of a dwell time map and improves its adaptability in the practical CCOS process. GEANS provides a novel method to compose the influence function matrix for multiple TIFs. It not only improves the computational efficiency of CNS by a factor of 1000, but also induces the optimized dwell time map to be smooth and have similar structure to the target removal map. The Genetic Algorithm (GA) is used to globally optimize the detailed parameters related to CNC dynamics limitations such as local slope of the dwell time. It also promotes the optimization results to have preferred characteristics that are mentioned above while achieving high figuring efficiency. These features enable to find desirable and practical dwell time maps for CCOS process.

The rest of the paper is organized as follows. The theoretical backgrounds for NS dwell time optimization and genetic algorithm are briefly reviewed in Section 2. In Section 3, we introduce GEANS method in detail. Section 4 presents the simulation results and the performance comparison between CNS and GEANS. Section 5 discusses the limitations of the proposed method, and Section 6 summarizes the implications of GEANS and concludes the paper.

2. Background

2.1. Non-sequential dwell time optimization

The purpose of dwell time optimization is to find a removal map, $z(x, y)$, which is close or equal to the target removal map, $z_d(x, y)$. Derived from the Preston equation [29], the material removal process in CCOS has been modeled as the convolution of a TIF, $t(x, y)$, with the corresponding dwell time, $d(\xi, \eta)$. When the sampling has finite resolution, the convolution process can be represented in matrix form as

$$z(x_k, y_k) = \sum_{i=1}^{N_d} t(x_k - \xi_i, y_k - \eta_i) d(\xi_i, \eta_i) \quad (1)$$

for $k = 1, 2, \dots, N_z$, where N_z is the number of sampling points in $z(x_k, y_k)$, N_d is the number of dwell points, (ξ_i, η_i) is the i th dwell point, and $t(x_k - \xi_i, y_k - \eta_i)$ represents the material removed per unit time at point (x_k, y_k) when the TIF dwells at (ξ_i, η_i) . Depending on the tool path or available tool overhang distance, (x_k, y_k) and (ξ_i, η_i) coordinates can be different. Equation (1) can also be represented as

$$\underbrace{\begin{pmatrix} z_1 \\ z_2 \\ \vdots \\ z_{N_z} \end{pmatrix}}_{\mathbf{z}} = \underbrace{\begin{pmatrix} t_{1,1} & t_{1,2} & \dots & t_{1,N_d} \\ t_{2,1} & t_{2,2} & \dots & t_{2,N_d} \\ \vdots & \vdots & \ddots & \vdots \\ t_{N_z,1} & t_{N_z,2} & \dots & t_{N_z,N_d} \end{pmatrix}}_{\mathbf{t}} \underbrace{\begin{pmatrix} d_1 \\ d_2 \\ \vdots \\ d_{N_d} \end{pmatrix}}_{\mathbf{d}} \quad (2)$$

where \mathbf{z} represents material removal map, \mathbf{t} represents influence function, and \mathbf{d} represents dwell time of each dwell point in matrix form. Since the convolution result between a dwell time basis, which is a group of tool location points with relative weights, and a TIF will compose a row of \mathbf{t} , it would be a sparse matrix that most elements of \mathbf{t} are zero except the convolution area.

In large optics fabrication, multiple TIFs are combined with different tool paths to achieve the desired residual error, $z_r(x, y) = z_d(x, y) - z(x, y)$, in the shortest available overall polishing time. In a previous study [19], we proposed the NS technique that counts multiple TIFs simultaneously in a single optimization process, which can be expressed as

$$z(x_k, y_k) = \sum_{j=1}^{N_t} \sum_{i=1}^{N_d^j} t_j(x_k - \xi_{j,i}, y_k - \eta_{j,i}) d_j(\xi_{j,i}, \eta_{j,i}) \quad (3)$$

where N_t is the number of TIFs, $(\xi_{j,i}, \eta_{j,i})$ represents the i th dwell point on the tool path of the j th TIF, and N_d^j is the number of total dwell points for the j th TIF. Each TIF has its own dwell time map, and the dwell points of each TIF can be varied when necessary. By considering multiple TIFs in optimization, the NS can achieve more balanced dwell time maps for each TIF to enhance CCOS efficiency than those optimized in the sequential way. Equation (3) can be represented as

$$\mathbf{z} = \left[\mathbf{t}_1, \dots, \mathbf{t}_{N_t} \right] \left[\mathbf{d}_1, \dots, \mathbf{d}_{N_t} \right]^T \quad (4)$$

In Eq. (4), as the NS method utilizes multiple tools, multiple influence matrices (\mathbf{t}_{N_t}) and corresponding dwell time matrices are included in the calculation.

Additionally, we can add alignment terms, such as piston, tip and tilt, to the target removal amount and run optimization. This process can be expressed as

$$z(x_k, y_k) = \sum_{j=1}^{N_t} \sum_{i=1}^{N_d^j} t_j(x - \xi_{j,i}, y - \eta_{j,i}) d_j(\xi_{j,i}, \eta_{j,i}) + \sum_{l=1}^{N_a} a_l(x, y) \quad (5)$$

where N_a is the number of optimized alignment terms and $a_l(x, y)$ is adjusted amount of the l th term. Considering the solution of a dwell time map must be non-negative in CCOS processes, the alignment terms help relax this constraint in the optimization, although the total dwell time may slightly increase.

The optimized dwell time map \mathbf{d}_{opt} is calculated as

$$\begin{aligned} \mathbf{d}_{opt} = \min_{\mathbf{d}, \mathbf{a}} \|\mathbf{t}\mathbf{d} - (\mathbf{z}_d + \mathbf{a})\|_2^2 \\ s.t. \mathbf{d} \geq \mathbf{0} \end{aligned} \quad (6)$$

where \mathbf{z}_d , represent the target removal map and \mathbf{a} represents adjusted alignment map. The amount of alignments will be calculated and optimized to minimize residual figure error. Therefore the estimated residual error map, \mathbf{z}_f , can be represented as

$$\mathbf{z}_f = \mathbf{z}_d - \mathbf{t}\mathbf{d}_{opt} - \mathbf{a} \quad (7)$$

2.2. Genetic algorithm

A GA is an evolutionary algorithm that models processes of natural selection to search a globally optimized solution [30,31]. It finds an optimized solution set (*i.e.*, chromosome) which is encoded in a sequence of numbers that representing optimizing parameters (*i.e.*, gene) among given parameter candidates (*i.e.*, gene pool). Each chromosome of a population is evaluated by predefined fitness function. The next generation of population is created through following genetic operations. To prompt the evolution path towards as our preference, those operations are based on the fitness. Chromosomes with higher fitness score has more probability to be mated (selection) and transfer their genes to the next generation by exchanging genes (crossover). Especially, chromosomes which have the highest fitness can be carried to the next generation directly (elitism) to keep the superiority. While exchanging genes, some of genes can be randomly selected and changed to others with a certain probability (mutation). Often, immigrants are joining to the next generation to keep the diversity in population. Over generations, the chromosomes are evolving toward the optimal solution until the maximum number of generation.

The GA has a high potential in solving complex problems such as dwell time optimization in CCOS process. For example, we can guide the optimization result to reflect our preference using the fitness function with preferred target criteria. Besides, if the gene pool has practical machining parameters only, the optimized dwell time map will be achievable solution in consequence. Thus, the GA enables us to find optimal combination of parameters while considering machining feasibility or our preference in CCOS process.

3. Genetic algorithm-powered non-sequential dwell time optimization

Our previously proposed CNS method [19] has shown the performance improvement in figuring efficiency compared to the sequential optimization. The optimized dwell time map from CNS, however, has issues when applying it in a laboratory setting. Firstly, the hardware capabilities are not reflected during the calculation. The applicable maximum local slope of dwell time map is limited due to the finite acceleration of machine. Hence a smooth dwell time map is preferred in actual CCOS processes, yet is not considered machine axis motion in CNS. Secondly, the calculated dwell time map barely resembles the target surface error map shape. Because of uncertainties in tool positioning and tool vibration, a dwell time map that is different from the target removal map increases the risk of inducing new surface error after figuring. Lastly, as the size of the influence matrix is multiplied by the number of TIFs in CNS, the computation time rises considerably. Especially in large optics fabrication (*e.g.*, GMT 8.4 m diameter mirror segment), the computational burden is even heavier since the sizes of measured removal maps and TIFs are enormous.

The main objectives of GEANS is to enhance the performance of CNS to produce a preferable dwell time map which closely duplicates the shape of a target error map and reflects the machining capability of the CNC unit while boosting the computational efficiency. GEANS consists of two interdependent parts: Composing the bases of the influence function matrix, and optimizing the dwell time using those bases via GA. Details of GEANS are explained in the rest of this section.

3.1. Set up the bases of influence function matrix

As Eq. (3) is usually ill-posed, finding the dwell time map relies on an optimization process. Constructing proper building blocks of the influence function matrix enables the optimization algorithm to find desired results easily and improves computational efficiency. We set up dwell time bases using following fundamental rules: i) grouping ii) dividing and iii) smoothing. Because each TIF has its own dwell time map in NS, the following process would be applied to each TIF case independently as well.

The first step is to form a single dwell time basis by grouping neighboring dwell points with similar removal amount. The idea of grouping is valid as adjacent dwell points with similar target removal amounts are expected to require similar dwell time distribution as well. It also benefits in computing costs as the total size of dwell time matrix is decreased. For instance, if n -points are combined and worked as a single dwell basis, the size of dwell time matrix is reduced by $n - 1$. Then, if the size of a single basis is too large, the optimization engine would not have enough degree of freedom in solution space. Therefore, in the algorithm, a criterion is set and a big single basis will be divided into smaller pieces to secure flexibility in optimization so that the overall figuring efficiency can be improved. A Smoothing filter is applied to all dwell time bases that are generated from above steps. We applied the Gaussian smoothing filter in GEANS to prevent sharp features and impose constraints on the local slope of the dwell time map. In addition, smoothing prevents square-wave like dwell time solutions from grouping and dividing processes and provides more reasonable solutions. After all, the convolution between each dwell time basis and TIF forms the influence matrix (\mathbf{t}) from Section 2. Through these processes, as the dwell time basis is more chunky and smooth than that of CNS, we can expect the result dwell time map would be less pointy than CNS. Figure 1 illustrates the process of making influence matrix.

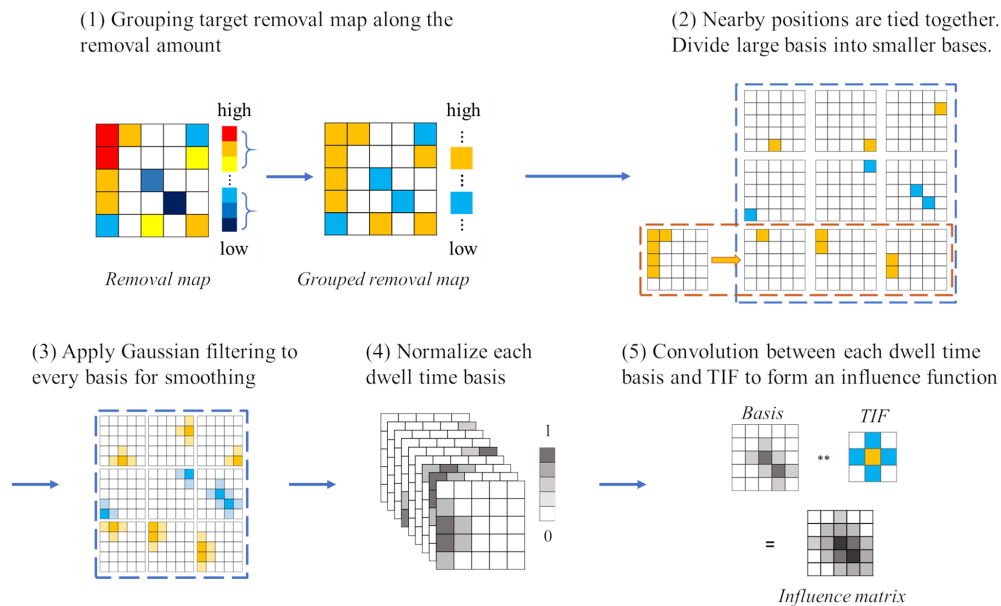


Fig. 1. The flowchart of generating an influence matrix. Specific figures relate to each step, such as the number of groups at step will be optimized through GA. The detailed explanations are illustrated in Fig. 2 in the following section.

3.2. Optimization parameters to construct influence function matrix

By leveraging GA, we can find optimal parameter sets for the influence function matrix and GEANS to generate a dwell time map while reflecting our preference in solution.

To implement GA, we need to define the parameters to be optimized (genes) and solution space (gene pool) first. In the case of GEANS, the parameters related in making influence matrix, explained in Section 3.1, comprise genes. Then the gene pool is built within the range available to the machine to assure the feasibility of a dwell time map. The gene pool should be wide enough to not restrain a possible solution space too hard, but at the same time, should not be too wide for efficient optimization.

The dwell position of a tool is another essential parameter to be determined. Since the accessible dwell points are limited by tool size and motion, a smaller size tool is advantageous to edge-side fabrication of the workpiece in general. Therefore, in our application of GEANS, we limited the coverage of the smallest tool to edge-side only to find reasonable balance between total fabrication time and remaining surface error. The applied parameters are summarized in Fig. 2.

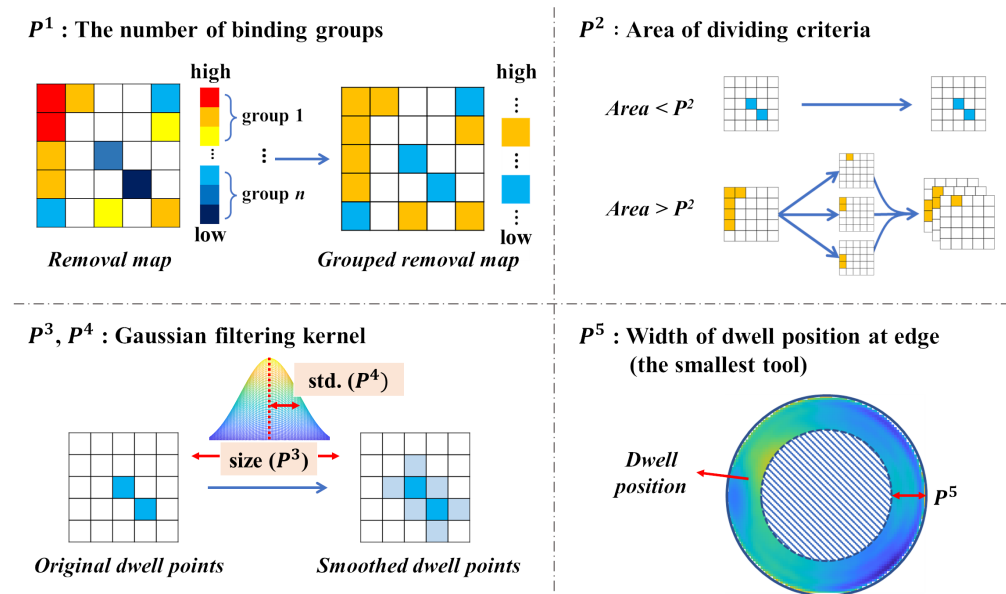


Fig. 2. Parameters to be optimized through genetic algorithm. For GEANS, the number of optimization parameters is multiplied with the number of TIFs. Note that P^1 and P^2 are simulation-related parameters while P^3 , P^4 and P^5 are tool-related parameters which are determined by machining capabilities.

3.3. Optimization and fitness function

Setting an appropriate fitness function is critical to lead the evolution of GA for our needs. The valid dwell time map in CCOS should duplicate the target removal map shape while achieving high figuring efficiency. Therefore, we evaluated the performance of the dwell time map with two indices: figuring efficiency and structural similarity.

Figuring Efficiency (FE) represents the accuracy of the algorithm for a given target removal map. The FE is defined as

$$FE(\mathbf{z}_d, \mathbf{z}_f) \equiv \frac{RMS[\mathbf{z}_d] - RMS[\mathbf{z}_f]}{RMS[\mathbf{z}_d]} \quad (8)$$

where RMS means Root Mean Squared value of each map. FE varies from 0 to 1, and a higher value means better figuring performance.

The Structural SIMilarity (SSIM) [32] is a quantified index to represent the visual similarity between two signals, μ_A and μ_B , by comparing luminance (l), contrast (c), and structural information (s). SSIM score varies from 0 to 1, and higher score means better similarity. The SSIM equation is represented as

$$SSIM(\mu_A, \mu_B) = l(\mu_A, \mu_B) \cdot c(\mu_A, \mu_B) \cdot s(\mu_A, \mu_B) \quad (9)$$

This index can be utilized to evaluate the validity of the dwell time map in CCOS since the valid dwell time map should closely copy the shape of the target removal map. We represent SSIM index between the normalized target error map and dwell time map of a TIF as

$$S_k(\mathbf{z}_d^{norm}, \mathbf{d}_k^{norm}) \equiv SSIM(\mathbf{z}_d^{norm}, \mathbf{d}_k^{norm}) \quad (10)$$

where \mathbf{z}_d^{norm} and \mathbf{d}_k^{norm} represent normalized target error map and dwell time map of k th TIF.

With FE and S_k , we form the fitness function (Q) as

$$Q(FE, S_k) = \frac{FE + \sum_{k=1}^l w_k \cdot S_k}{1 + \sum_{k=1}^l w_k} \quad (11)$$

where w is relative weight of SSIM of each TIF case compared to FE. Note that the w has no general solution for the simulation, and can be changed based on the priority of the optimization result or machining capability.

The whole process of GEANS simulation is shown in the following Fig. 3.

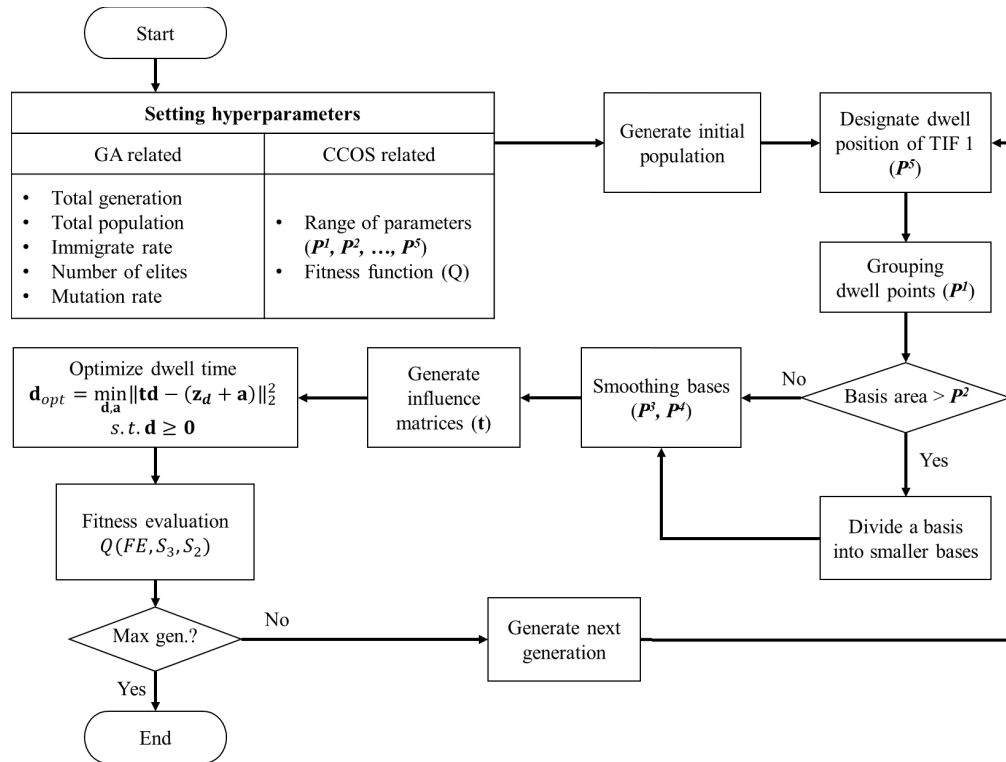


Fig. 3. Flowchart of GEANS simulation.

4. Verification of GEANS through simulations

4.1. CCOS simulation setup

We performed CCOS simulation to verify the performance of GEANS compared to CNS. We employed actual measurement data of the target removal map (Fig. 4), and TIF data for a more realistic simulation. The target workpiece was a mirror, 4.25 m in diameter with an initial RMS surface figure error of 0.749 μm . The target removal map was 341 by 341 pixels with a 12.5 mm pixel scale.

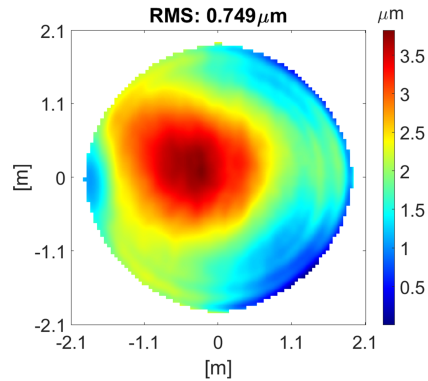


Fig. 4. Target removal map for CCOS simulation. RMS of surface figure error is 0.749 μm .

Three different TIFs were used for the simulation. The radius of orbital stroke TIFs [29] were 100 mm (TIF 1), 250 mm (TIF 2), and 400 mm (TIF 3) respectively. Due to the limited overhang ratio, we assumed that TIF 2 and 3 cannot travel farther than 100 mm (8 pixels) from the edge.

Defining the proper range of our parameters and hyperparameters are important to induce the desired result from GEANS. It is worthy to note that the used range of optimization parameters and hyperparameters can be varied upon the CCOS circumstances of users based on their target removal map, practical limitations (*e.g.* maximum tool size and weight), available polishing resources (*e.g.* sufficient and stable polishing compound supply chain, available pitch types), or achievable machining specifications (*e.g.* maximum motor speed, gear wear). For hyperparameters related to GA, we set the maximum generation number to 20, and each generation consists of 50 chromosomes. Among 50 chromosomes, 5 chromosomes were from the previous generation which scores high, 30 chromosomes were children that formed through crossover with a random multiplication rate of 0.3, and 15 chromosomes were new immigrants.

Domains of parameters illustrated in Section 3.1 is another critical part to improve the performance of GEANS, yet the general solutions do not exist. In this simulation, we set the domains of each parameter empirically as summarized in Table 1.

As the smallest TIF (TIF 1) is dedicated to edge area only, we take into account the SSIM index of TIF 2 and 3 in the fitness function. Although multiple TIF sizes will be optimized simultaneously in GEANS, the actual polishing runs will remain sequential (*e.g.*, from larger to smaller tool sizes). We set higher weight to the TIF 3 than TIF 2 in the simulation. The fitness function we used here is

$$Q(FE, S_3, S_2) = \frac{FE + 5 \cdot S_3 + 2 \cdot S_2}{8} \quad (12)$$

The simulations were performed with MATLAB version 2021a on a desktop equipped with AMD Ryzen 9 3950X (16 cores, 3.5 GHz) and 128 GB RAM.

Table 1. Ranges of parameters to be optimized through GA. These values are determined empirically. Numbers in brackets represent the range of each parameter. For example, [5:5:30] means [minimum : steps : maximum].

	TIF 1	TIF 2, 3
P ¹ (px.)		[5:5:30]
P ² (px. ²)	[1000:200:2000]	[20000:20000:120000]
P ³ (px.)		[13×13]:[4×4]:[29×29]
P ⁴ (px.)		[1:1:4]
P ⁵ (px.)	[5:5:30]	N.A

4.2. Simulation results

4.2.1. Simulation result from CNS

We baseline our performance with the results of the CNS algorithm. In the simulation, we assume the dwell points are equal to the sampling points, and the raster tool path is used while this can be any other tool path (*e.g.*, spiral) according to the actual machine's configuration. Note that the CCOS simulation conditions were mostly identical between CNS and GEANS except for the constraints of TIF 1 and the spatial resolution of data. Due to the high memory occupation, we needed to use less sampled data that has half the spatial resolution (171 by 171) in CNS. The computing efficiency between algorithms is summarized at Table 2 in the following chapter.

Table 2. Computing speed comparison between GEANS and CNS.

Method	Map size [px.]	Size of $t_{m \times n}$	$m \times n$	Computation [s]	FE [%]
GEANS	341 × 341	72641×3681	267,391,521	Single: 24.4 Total: 22,082	94.3
GEANS (Low samp.)	171 × 171	18317×3898	71,399,666	Single: 4.9 Total: 4,437	94.4
CNS (Low samp.)	171 × 171	18317×51423	941,915,091	5,131	98.0

Figure 5 shows the dwell time maps of each TIF and remaining error map after applied each dwell time map from CNS method. In this simulation, we assumed TIFs were applied sequentially from TIF 3 to TIF 1. The adjusted alignment amounts for CNS were $-0.86 \mu\text{m}$ of piston, $6.57 \times 10^{-5} \text{mrad}$ in x-tilt and $-3.04 \times 10^{-4} \text{mrad}$ in y-tilt. The RMS of residual surface error (Fig. 5(f)) is about 15 nm which corresponds to 98 % of FE. Although CNS shows very high FE, the outcome dwell time maps have several point-like, disconnected spots (top row of Fig. 5). These dwell time maps are not preferred in actual CCOS running because the machine requires high acceleration and deceleration. It usually requires the post-processing to translate dwell time maps into affordable machine motion, and it induces the unexpected error on final outcome. Besides, the dwell time maps barely followed the shape of target removal map, so that the risk of inducing unexpected spatial frequency errors on residual surface is high. Therefore the results from CNS have limited potential for practical implementation.

4.2.2. Simulation result from GEANS

Figure 6 shows the result of GEANS. Similar to CNS, the dwell points were equal to the sampling points. In GEANS, however, the smallest tool (TIF 1) only covers the area determined by P⁵ as illustrated at Section. 3.2, and the sampling interval is 12.5 mm which yields double resolution of CNS. After optimization the RMS of the residual surface error was 0.043 μm which corresponds to 94.3% of FE. Adjusted alignment amounts were $-1.26 \mu\text{m}$ of piston, $-1.46 \times 10^{-6} \text{mrad}$ in x-tilt and $1.79 \times 10^{-5} \text{mrad}$ in y-tilt. Compared to CNS, the FE value was dropped 3.7 percentage points but still reasonably high FE. In terms of similarity of dwell time map, dwell time map of

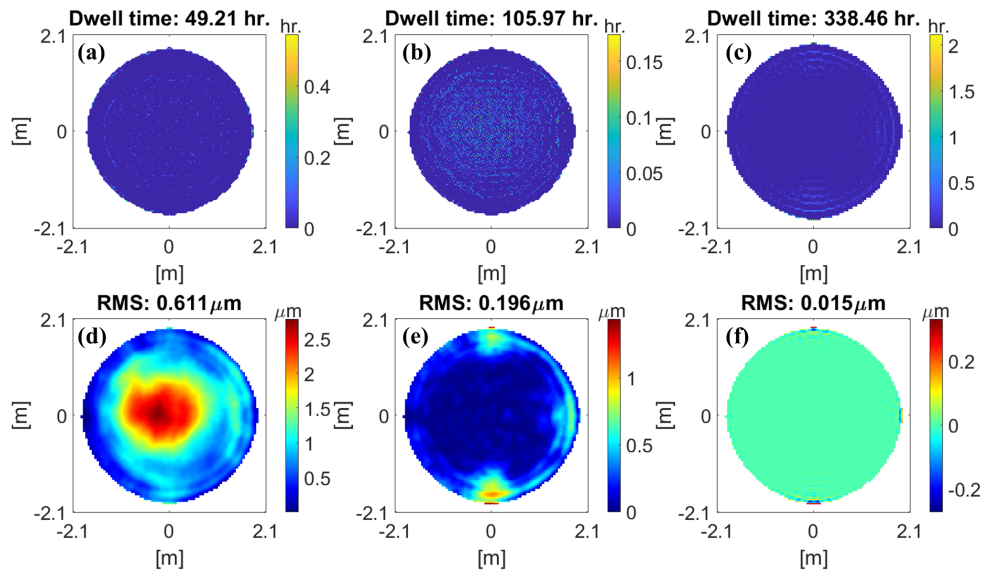


Fig. 5. CNS results dwell time maps and residual error maps. Dwell time map of (a) TIF 3 (b) TIF 2 and (c) TIF 1. Surface error maps after applying (d) TIF 3 (e) TIF 2 and (f) TIF 1 sequentially. Residual surface figure error after CNS was about about 15 nm.

TIF 3 (Fig. 6(a)) and 2 (Fig. 6(b)) closely replicate the shape of target removal map (Fig. 4) as we intended. The SSIM indices of each tool are 0.91 for TIF 3 and 0.85 for TIF 2.

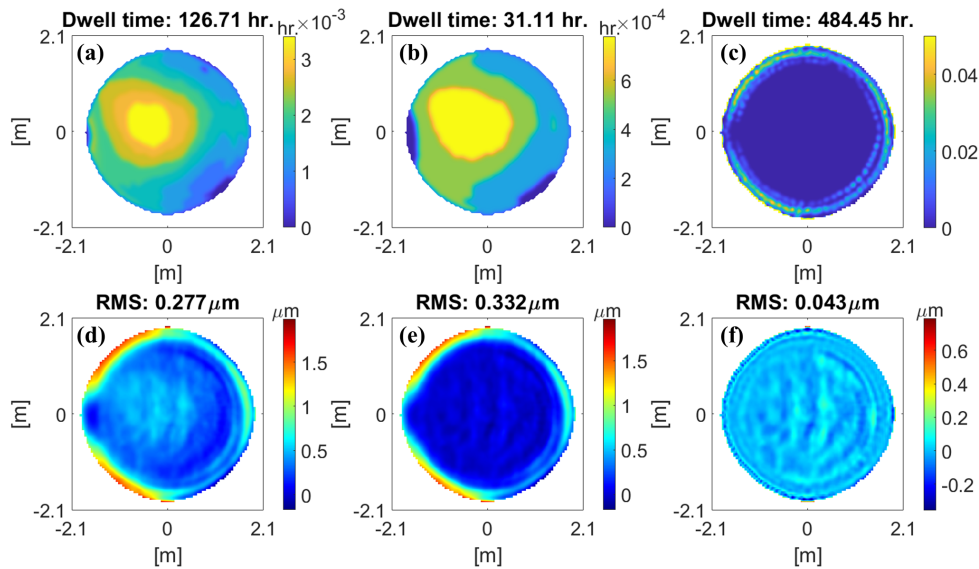


Fig. 6. Resulted maps from GEANS. Dwell time maps of (a) TIF 3 (b) TIF 2 (c) TIF 1. Residual surface error maps after applying (d) TIF 3 (e) TIF 2 and (f) TIF 1 in sequentially. Residual error map of GEANS was 43 nm of RMS.

Figure 7 shows how the fitness function, RMS of residual surface error, and similarity of TIF 2 and 3 were changed over 20 generations. The RMS and similarity values were from the chromosome which has the highest score in that generation. Though the RMS of the residual

map and both SSIM do not monotonically decrease or increase, the fitness function increases as the generations pass.

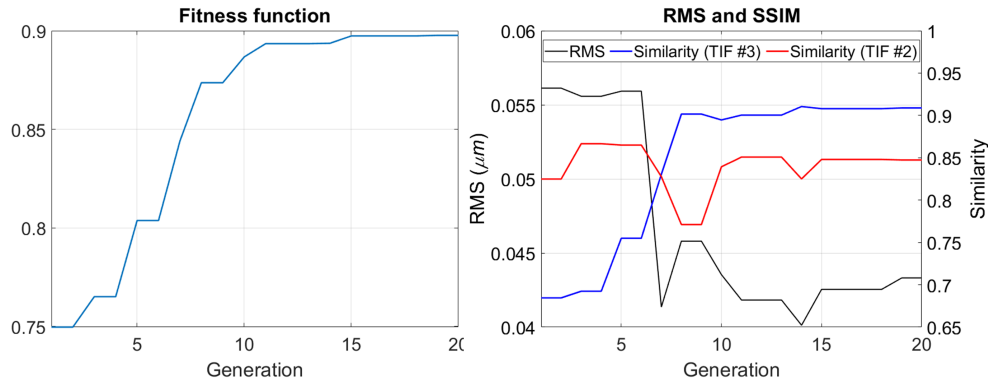


Fig. 7. (Left) Fitness function value over 20 generations of evolving. (Right) RMS of remained surface error and S_2 and S_3 of each generations. The transformation of TIF 3 over generations is shown in [Visualization 1](#).

4.3. Validation of GEANS

Compared to CNS, GEANS shows enhanced practicality of dwell time maps through three main features: building the influence matrix, smoothing dwell time maps, and employing SSIM index to make dwell time map to copy the shape of target removal map. In this chapter, we analyze how these aspects affect GEANS's performance.

Since GEANS utilized a GA that requires large number of repeated optimization calculations, improved computing efficiency was essential. By grouping and dividing, GEANS cuts down the size of elements of the influence function (\mathbf{t}) to more than 10 times smaller than CNS at the same resolution (Table 2) while maintaining enough degrees of freedom in optimization for figuring efficiency. As a result, GEANS shows 1000 times optimization speed increase for a single optimization on average. The total calculation time was shorter yet, as GEANS required 905 (50 times from the first generation, and 45 times from the rest generations) iterative optimizations. It also enables us to use higher resolution data which benefits in large optics fabrication. Even with higher resolution, the size of influence matrix of GEANS is smaller so that the single computation took still less time than CNS.

Smoothing with Gaussian filtering also increased practicality of dwell time maps from GEANS. Figure 8 shows the resulted dwell time map of TIF 3 from GEANS when smoothing was applied (Fig. 8(a)) and was not (Fig. 8(b)). Without smoothing, the slope of dwell time change was abruptly between adjacent well points. Further the dwell time map was less similar ($S_3 = 0.59$) to the shape of target removal map than GEANS result ($S_3 = 0.91$).

SSIM also has an important role to produce desirable dwell time map in GEANS. Figure 9 shows the obtained dwell time maps of TIF 3 with and without SSIM index in the fitness function. Without SSIM (Fig. 9(b)), dwell time map is not duplicating the target removal map noticeably. Besides, some dwell points were not linked together and slope of dwell time map is steep which causes inessential acceleration of tool (Fig. 9(c)).

4.4. Error analysis of dwell time maps

Simulation results are degraded while applying in actual CCOS process due to various error sources which include tool positioning error, random variation in TIF, limited acceleration of

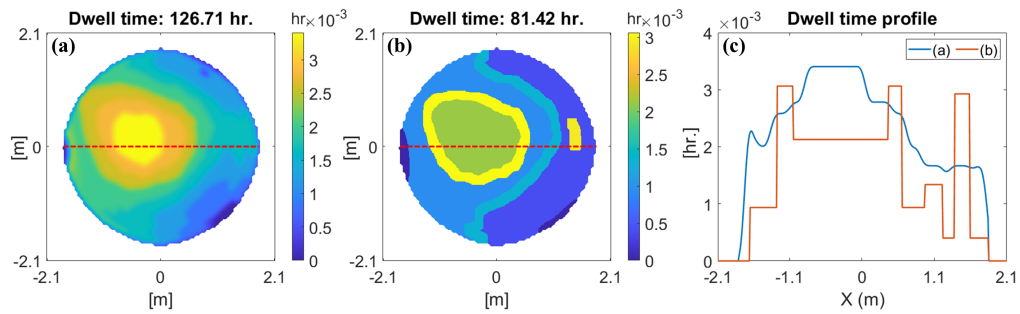


Fig. 8. Comparison of dwell time map to show smoothing affects. Dwell time map of TIF 3 are shown here. (a) GEANS (b) GEANS without smoothing. (c) Center line profile (Red dotted lines in (a) and (b)) of each dwell time map.

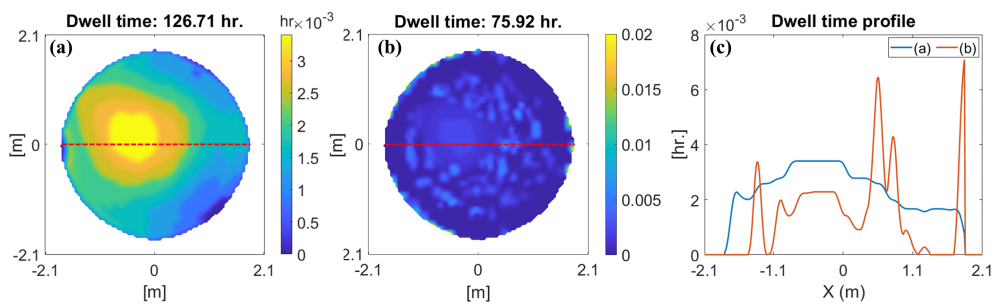


Fig. 9. Dwell time maps of TIF 3 when SSIM was (a) considered and (b) not considered in fitness function. Without SSIM, the resulted dwell time map was neither copying the shape of target removal map and smoothly continuous. (c) Center line profile (Red dotted lines in (a) and (b)) of each dwell time map.

tool, or laboratory environment. Considering these factors, we implemented robustness test to compare the stability and usability of dwell time maps from GEANS and CNS.

First, we imposed random errors to dwell position and TIF and checked how the Power Spectral Density (PSD) is changed. Both random error had rectangular distribution function of which boundary values were up to ± 10 mm for tool positioning errors and $\pm 10\%$ for TIF value errors. Within the boundary, random errors were added or subtracted from the original dwell time. Figure 10 shows the variation of PSD with perturbations. Without error (thick blue lines in the figure), the CNS method (Fig. 10(b)) shows lower PSD in overall frequency than GEANS (Fig. 10(a)). However, with perturbations, PSD of CNS was changed and distributed broadly while PSD of GEANS was remained stable. These results implied that GEANS result is more predictable and robust against to the given errors so that more applicable than CNS in actual CCOS operation.

We then evaluated applicability of dwell time maps from each method. In actual CCOS running, since the maximum acceleration of tool is limited, dwell time maps that have smooth slopes along tool path are preferred and feasible solutions. Especially in large optics fabrication, as the sizes of tools are larger, controlling the tool acceleration is getting more difficult. Figure 11 is a histogram showing distribution of dwell time slopes of TIF 2 and TIF 3 from GEANS and CNS. As expected, slopes of CNS were higher than GEANS in general.

We investigated how the limited acceleration affects the residual error map. We employed the continuous raster motion tool path, and set limits in dwell time difference along the path. If the difference is larger than the set limit, the dwell time limit is added or subtracted to an adjacent

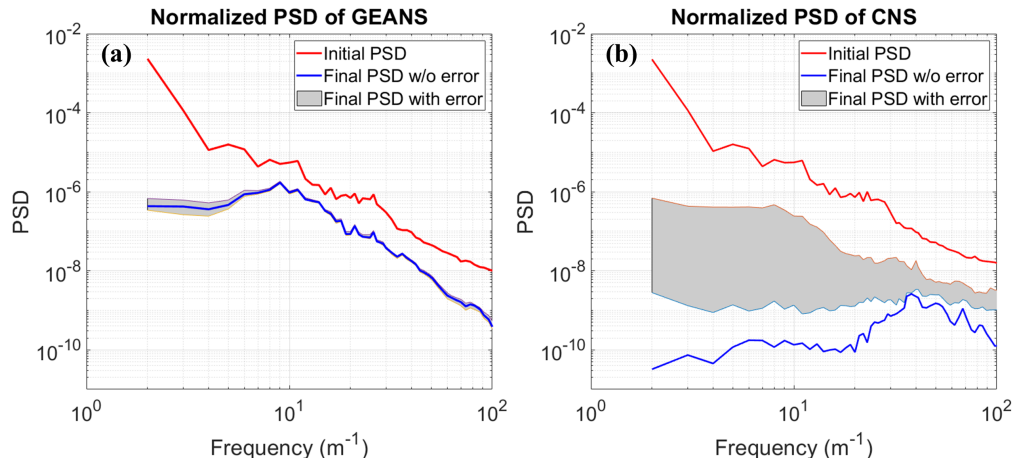


Fig. 10. Compared PSD of remained surface error map after considering practical operation of (a) GEANS method and (b) CNS method. PSD of GEANS was remained steady while the PSD of CNS was worsened with perturbation.

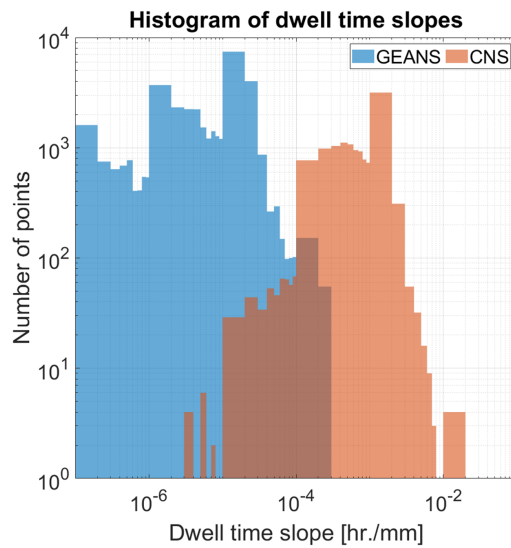


Fig. 11. Histogram of dwell time slopes. X and Y axis are represented in log-scale. This different distribution in slopes of each method implies that the required maximum acceleration for GEANS is lower than CNS.

dwell point along the tool path until every difference is under the limit. Assuming the TIF 1 can have higher acceleration, this adjustment is applied to TIF 2 and 3.

We applied various slope limitations from 10^{-2} mm/hour to 10^{-5} mm/hour and analyzed how the dwell time maps and residual maps were changed. Figure 12 shows how the dwell time map of TIF 3 is changed when the maximum slope is limited to 0.001 mm/hour. In CNS, compared to the original map (Fig. 12(a)), dwell points with steep slopes were elongated and in consequence total dwell time was increased (Fig. 12(b)). GEANS, on the other hand, had no change in dwell time maps from the initial results since most of dwell points were already within the limit (Fig. 12(c), (d)).

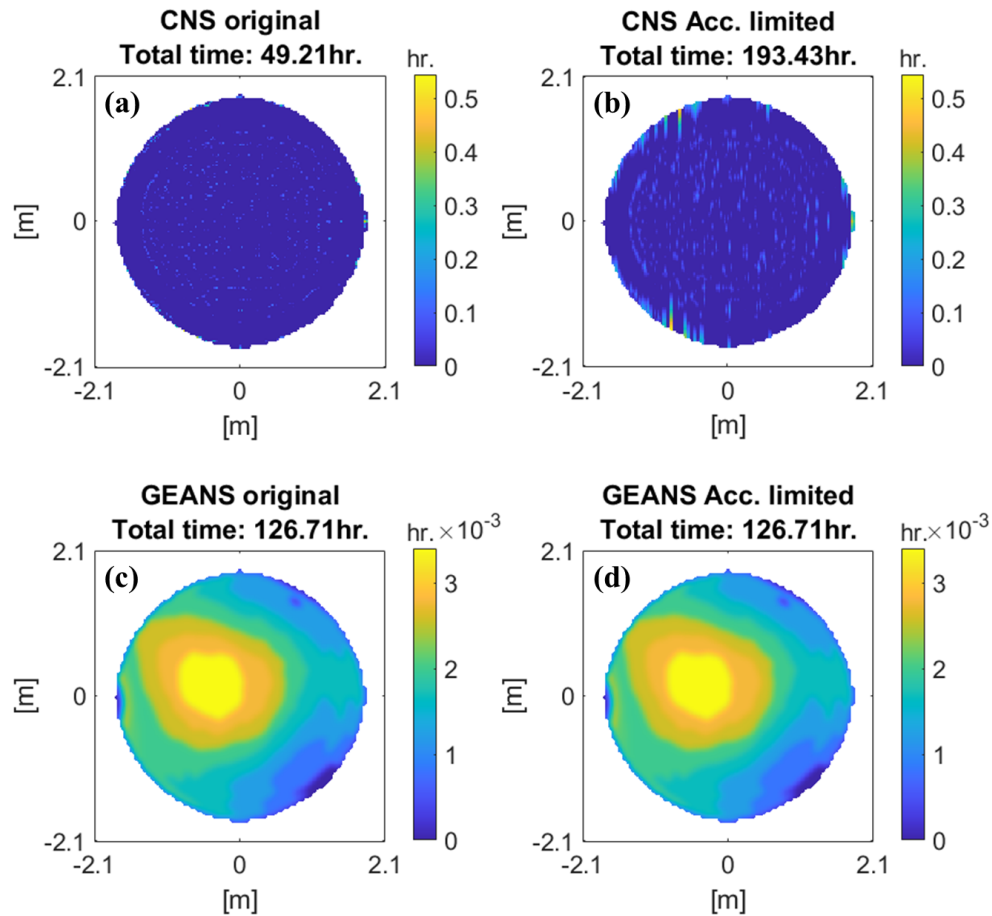


Fig. 12. Variation of dwell time map when the acceleration limit (0.001 mm/hour) is applied. (a) Original dwell time map of TIF 3 from CNS and (b) Dwell points with high slopes were adjusted. As dwell time map was smoothed, total dwell time was extended as well. (c) Original dwell time map of TIF 3 from GEANS. (d) Slope limitation was applied but no difference in dwell time map.

The variation in dwell time maps, of course, affect to the final CCOS results as well. Figure 13 shows how the residual error map changed due to acceleration limitations. The FE of CNS was rapidly worsening because the dwell time maps could not be applied as optimized yet the results from GEANS remained stable. The effects of other maximum slope cases are shown in [Visualization 2](#) for GEANS case and [Visualization 3](#) for CNS case.

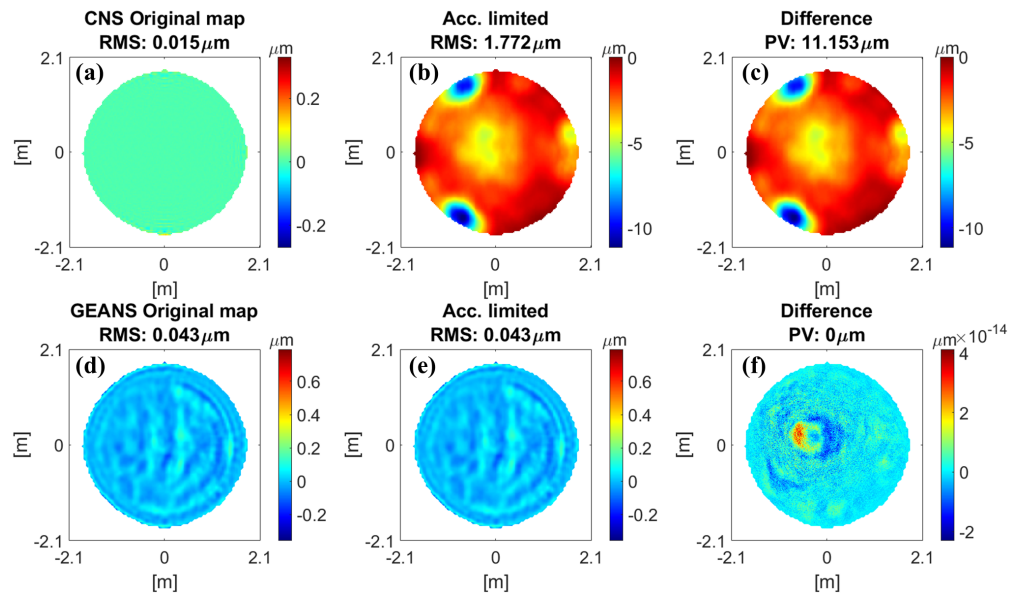


Fig. 13. Changes of residual error map when the acceleration limit was applied. (a) Original result from CNS. (b) Residual map when maximum acceleration was applied (CNS). (c) Difference map between (a) and (b). (d) Original result from GEANS. (e) Residual map when maximum acceleration was applied (GEANS). (f) Difference map between (d) and (e).

5. Discussion

The increased residual RMS and total dwell time in GEANS compared to CNS. It is also worth mentioning that, although CNS showed better initial results than GEANS in simulation, the results from CNS have limited potential for practical implementation as the results from CNS are very sensitive to common errors in CCOS process (*e.g.* tool positioning, TIF model accuracy) or machine capabilities (*e.g.* tool acceleration limits). For example, the total dwell times of each CNS (Fig. 5) and GEANS (Fig. 6) were 494 hour and 642 hour respectively. Also the residual RMS of CNS ($0.015 \mu\text{m}$) was lower than that of GEANS ($0.043 \mu\text{m}$). However, with machining errors, the outcome from CNS is less predictable than that of GEANS (Fig. 10). Further, when we consider the limit in tool acceleration as shown in Figs. 12, 13 and Visualization 3, the total run time of CNS will be increased notably as well as the estimated residual RMS unless the CCOS machine can meet the rapid motion limit which is not easy to be achieved especially for large optics fabrication tools.

6. Conclusion

In this paper, we proposed a novel dwell time optimization method called GEANS (Genetic algorithm-powered non-sequential), which can combine the modern numerical optimization computing power and the skilled human expert's brain power (*e.g.*, optician's intuitive dwell time estimation). To provide practical and applicable dwell time map solution, we built an influence matrix through grouping, dividing, and smoothing procedures. In this process, excessive number of parameters were needed to be optimized such as criteria of grouping and dividing, and the size of Gaussian smoothing filter. However, the correlation between parameters and final dwell time map was not easy to identify mathematically. Therefore, we employed genetic algorithms to find optimal parameters associated with influence matrix. The performance of GEANS was demonstrated with CCOS simulation using the real surface error map and TIF data. Compared

to CNS, GEANS achieved comparable FE (94.3 %) and 1000 times faster computation speed. Further, the result dwell time maps were closely reproduced the shape of target removal map which are preferable in actual CCOS running. Error analyses were also performed to demonstrate the stability and applicability of each algorithm. Up to 10 mm of tool position and 10 % of TIF were perturbed and checked impact in PSD. Results showed that dwell time maps from GEANS were remarkably more practicable and stable than those of CNS in given perturbations. We also applied maximum achievable tool acceleration and examined how dwell time maps and final residual surface error maps were changed. The GEANS dwell time maps were smooth and continuous compared to CNS, which allowed much slower tool acceleration to complete calculated dwell time maps.

We believe that the flexibility and capability of being expanded adds more unique value to GEANS. The optimizing parameters can be included or withdrawn depending on the achievable system conditions. Further, beyond the dwell time, other CCOS items such as the tool path or types of TIF also can be optimized while reflecting the priorities of CCOS result in GEANS.

Acknowledgments. We also want to thank the people who contributed to the editing and reviewing of the manuscript. A special thank you goes to Jaren Ashcraft and Henry Quach who helped edit and gave feedback on the article.

Disclosures. The authors declare no conflicts of interest.

Data availability. Data underlying the results presented in this paper are not publicly available at this time but may be obtained from the authors upon reasonable request.

References

1. R. Aspden, R. McDonough, and F. R. Nitchie, "Computer assisted optical surfacing," *Appl. Opt.* **11**(12), 2739–2747 (1972).
2. R. Wagner and R. Shannon, "Fabrication of aspherics using a mathematical model for material removal," *Appl. Opt.* **13**(7), 1683–1689 (1974).
3. R. A. Jones, "Computer-controlled polishing of telescope mirror segments," *Opt. Eng.* **22**(2), 222236 (1983).
4. R. A. Jones, "Computer-controlled optical surfacing with orbital tool motion," *Opt. Eng.* **25**(6), 256785 (1986).
5. R. A. Jones and W. J. Rupp, "Rapid optical fabrication with CCOS," in *Advanced Optical Manufacturing and Testing*, vol. 1333 G. M. Sanger, P. B. Reid, and L. R. Baker, eds., International Society for Optics and Photonics (SPIE, 1990), pp. 34–43.
6. H. Pollicove and D. Golini, "Deterministic manufacturing processes for precision optical surfaces," in *Key Engineering Materials*, vol. 238 (Trans Tech Publ, 2003), pp. 53–58.
7. J. H. Burge, S. Benjamin, D. Caywood, C. Noble, M. Novak, C. Oh, R. Parks, B. Smith, P. Su, M. Valente, and C. Zhao, "Fabrication and testing of 1.4-m convex off-axis aspheric optical surfaces," in *Optical manufacturing and testing VIII*, vol. 7426 (International Society for Optics and Photonics, 2009), p. 74260L.
8. M. J. Valente, D. W. Kim, C. J. Oh, M. J. Novak, and J. H. Burge, "Fabrication of 4-meter class astronomical optics," in *Modern Technologies in Space- and Ground-based Telescopes and Instrumentation*, vol. 7739 E. Atad-Ettinger, D. Lemke, eds., International Society for Optics and Photonics (SPIE, 2010), pp. 880–892.
9. M. Johns, "The giant magellan telescope (gmt)," in *Ground-based and Airborne Telescopes*, vol. 6267 (International Society for Optics and Photonics, 2006), p. 626729.
10. J. Nelson and G. H. Sanders, "The status of the thirty meter telescope project," in *Ground-based and Airborne Telescopes II*, vol. 7012 (International Society for Optics and Photonics, 2008), p. 70121A.
11. T. Andersen, A. L. Ardeberg, J. Beckers, A. Goncharov, M. Owner-Petersen, H. Riewaldt, R. Snel, and D. Walker, "The euro50 extremely large telescope," in *Future Giant Telescopes*, vol. 4840 (International Society for Optics and Photonics, 2003), pp. 214–225.
12. A. Ardeberg, T. Andersen, J. Beckers, M. Browne, A. Enmark, P. Knutsson, and M. Owner-Petersen, "From euro50 toward a european elt," in *Ground-based and Airborne Telescopes*, vol. 6267 (International Society for Optics and Photonics, 2006), p. 626725.
13. R. A. Jones, "Optimization of computer controlled polishing," *Appl. Opt.* **16**(1), 218–224 (1977).
14. C. Wang, W. Yang, Z. Wang, X. Yang, C. Hu, B. Zhong, Y. Guo, and Q. Xu, "Dwell-time algorithm for polishing large optics," *Appl. Opt.* **53**(21), 4752–4760 (2014).
15. S. Wilson and J. McNeil, "Neutral ion beam figuring of large optical surfaces," in *Current Developments in Optical Engineering II*, vol. 818 (1987), pp. 320–325.
16. T. Wang, L. Huang, H. Kang, H. Choi, D. W. Kim, K. Tayabaly, and M. Idir, "RIFTA: A Robust Iterative Fourier Transform-based dwell time Algorithm for ultra-precision ion beam figuring of synchrotron mirrors," *Sci. Rep.* **10**(1), 8135 (2020).

17. T. Wang, L. Huang, H. Choi, M. Vescovi, D. Kuhne, Y. Zhu, W. C. Pullen, X. Ke, D. W. Kim, Q. Kemaoy, K. Tayabaly, N. Bouet, and M. Idir, "Rise: robust iterative surface extension for sub-nanometer x-ray mirror fabrication," *Opt. Express* **29**(10), 15114–15132 (2021).
18. C. L. Carnal, C. M. Egert, and K. W. Hylton, "Advanced matrix-based algorithm for ion-beam milling of optical components," in *Current Developments in Optical Design and Optical Engineering II*, vol. 1752 (1992), pp. 54–63.
19. D. W. Kim, S.-W. Kim, and J. H. Burge, "Non-sequential optimization technique for a computer controlled optical surfacing process using multiple tool influence functions," *Opt. Express* **17**(24), 21850–21866 (2009).
20. J. F. Wu, Z. W. Lu, H. X. Zhang, and T. S. Wang, "Dwell time algorithm in ion beam figuring," *Appl. Opt.* **48**(20), 3930–3937 (2009).
21. T. Wang, L. Huang, M. Vescovi, D. Kuhne, K. Tayabaly, N. Bouet, and M. Idir, "Study on an effective one-dimensional ion-beam figuring method," *Opt. Express* **27**(11), 15368–15381 (2019).
22. P. Ji, D. Li, X. Su, Z. Qiao, K. Wu, L. Song, B. Peng, and B. Wang, "Optimization strategy for the velocity distribution based on tool influence function non-linearity in atmospheric pressure plasma processing," *Precis. Eng.* **65**, 269–278 (2020).
23. A. Chernyshev, N. Chkhalo, I. Malyshev, M. Mikhailenko, A. Pestov, R. Pleshkov, R. Smertin, M. Svechnikov, and M. Toropov, "Matrix based algorithm for ion-beam figuring of optical elements," *Precis. Eng.* **69**, 29–35 (2021).
24. T. Wang, L. Huang, M. Vescovi, D. Kuhne, Y. Zhu, V. S. Negi, Z. Zhang, C. Wang, X. Ke, H. Choi, W. C. Pullen, D. Kim, Q. Kemaoy, K. Nakhoda, N. Bouet, and M. Idir, "Universal dwell time optimization for deterministic optics fabrication," *Opt. Express* **29**(23), 38737–38757 (2021).
25. C. Jiao, S. Li, and X. Xie, "Algorithm for ion beam figuring of low-gradient mirrors," *Appl. Opt.* **48**(21), 4090–4096 (2009).
26. H. Martin, R. Allen, J. Burge, D. Kim, J. Kingsley, M. Tuell, S. West, C. Zhao, and T. Zobrist, "Fabrication and testing of the first 8.4-m off-axis segment for the giant magellan telescope," in *Modern Technologies in Space-and Ground-based Telescopes and Instrumentation*, vol. 7739 (International Society for Optics and Photonics, 2010), p. 77390A.
27. J. H. Burge, D. W. Kim, and H. M. Martin, "Process optimization for polishing large aspheric mirrors," in *Advances in Optical and Mechanical Technologies for Telescopes and Instrumentation*, vol. 9151 (International Society for Optics and Photonics, 2014), p. 91512R.
28. C. J. Oh, A. E. Lowman, G. A. Smith, P. Su, R. Huang, T. Su, D. Kim, C. Zhao, P. Zhou, and J. H. Burge, "Fabrication and testing of 4.2 m off-axis aspheric primary mirror of daniel k. inouye solar telescope," in *Advances in Optical and Mechanical Technologies for Telescopes and Instrumentation II*, vol. 9912 (International Society for Optics and Photonics, 2016), p. 99120O.
29. D. W. Kim and S.-W. Kim, "Static tool influence function for fabrication simulation of hexagonal mirror segments for extremely large telescopes," *Opt. Express* **13**(3), 910–917 (2005).
30. J. H. Holland, *Adaptation in natural and artificial systems: an introductory analysis with applications to biology, control, and artificial intelligence* (MIT press, 1992).
31. K. A. De Jong, *An analysis of the behavior of a class of genetic adaptive systems*. (University of Michigan, 1975).
32. Z. Wang, A. C. Bovik, H. R. Sheikh, and E. P. Simoncelli, "Image quality assessment: from error visibility to structural similarity," *IEEE Trans. on Image Process.* **13**(4), 600–612 (2004).